A 3–5 μm broadband YBCO high-temperature superconducting photonic crystal

Gang Liu(刘刚)[1,2,†], Yuanhang Li(李远航)[2,3], Baonan Jia(贾宝楠)[2], Yongpan Gao(高永潘)[2], Lihong Han(韩利红)[2], Pengfei Lu(芦鹏飞)[2,3], and Haizhi Song(宋海智)[4,‡]

[1] *Beijing Key Laboratory of Space-Ground Interconnection and Convergence, Beijing University of Posts and Telecommunications, Beijing* 100876, *China*
[2] *School of Electronic Engineering, Beijing University of Posts and Telecommunications, Beijing* 100876, *China*
[3] *State Key Laboratory of Information Photonics and Optical Communications, Beijing University of Posts and Telecommunications, Beijing* 100876, *China*
[4] *Southwest Institute of Technical Physics, Chengdu* 610041, *China*

(Received 20 October 2022; revised manuscript received 31 December 2022; accepted manuscript online 31 January 2023)

Photonic crystal structures have excellent optical properties, so they are widely studied in conventional optical materials. Recent research shows that high-temperature superconducting periodic structures have natural photonic crystal features and they are favourable candidates for single-photon detection. Considering that superconductors have completely different properties from conventional optical materials, we study the energy level diagram and mid-infrared 3 μm–5 μm transmission spectrum of two-dimensional superconducting photonic crystals in both superconducting and quenched states with the finite element method. The energy level diagram of the circular crystal column superconducting structure shows that the structure has a large band gap width in both states. At the same fill factor, the circular crystal column superconducting structure has a larger band gap width than the others structures. For lattice structures, the zero transmission point of the square lattice structure is robust to the incident angle and environmental temperature. Our research has guiding significance for the design of new material photonic crystals, photon modulation and detection.

Keywords: high-temperature superconducting, mid-infrared, photonic crystal, single-photon detection

PACS: 42.50.–p, 42.70.Qs, 03.67.–a **DOI:** 10.1088/1674-1056/acb760

1. Introduction

Photonic crystals (PCs) are spatially periodic arrays composed of materials with different dielectric constants,[1–3] which have aroused great interest in the past decades for their ability to control light.[4,5] Their properties are determined by a combination of geometry and material properties, making them extremely customizable. The energy level diagram of PCs is similar to the electronic energy level diagram in crystal physics. PCs can be used to develop all kinds of sensors, such as biochemical sensors,[6–8] mechanical sensors,[9,10] temperature sensors,[11,12] refractive index sensors,[13,14] and gas sensors;[15,16] optical modulation devices, such as optical fibers,[17,18] waveguides,[19–24] optical filters,[25–27] and microcavities;[28–30] and single-photon detectors.[31–34] Photonic crystal structures have been extensively studied in traditional materials. In fact, many new materials have the natural photonic crystal structure, such as yttrium barium copper oxide (YBCO) high-temperature superconductors (HTSs), and it is also of great significance to study the properties of their photonic crystals in these new materials.

Superconductors, especially the HTSs of copper oxides, are promising materials for quantum information processing. The superconductivity of copper oxides can be easily realized by cooling to below the critical temperature, which is attractive for technical applications. Currently, research on copper oxide superconductors is not limited to the preparation of materials, and the design of the geometric structure has attracted more interest and achieved excellent results, such as nanopatterned YBCO thin films,[35–37] HTS and semiconductor combinations,[38] heterogeneous structures of metals and superconducting photonic crystals (SPCs),[39] and superconducting array structures.[40]

The study of SPCs[41] has attracted increasing attention due to their smaller incident scattering, temperature sensitivity, and magnetic field sensitivity.[42,43] Previous studies have focused on the properties of PCs in the superconducting state,[44] and there has little research on their quenched state. However, photon detection with superconductors will inevitably involve the properties of photons in the superconducting state and the quenched state, and the properties of SPCs in these two states must be detected. Therefore, the research on the properties of SPCs cannot be replaced by the research on photonic crystals of conventional materials.

In this paper, we design a YBCO SPC structure.[45] The photon response caused by geometric structure is very important, because it is related to whether photons can form coupling with Cooper pairs. The optical properties of the superconducting state and the quenched state[45] are calculated using the finite element method (FEM)[46–53] under the two-fluid model.[40,54] The band gap widths of the HTS PCs with

†Corresponding author. E-mail: liu_g@126.com
‡Corresponding author. E-mail: hzsong1296@163.com

© 2023 Chinese Physical Society and IOP Publishing Ltd

different superconducting structures, such as a circular crystal column structure, a square crystal column structure, and a rectangular crystal column structure, are calculated.[54] To ensure the accuracy of the study, we analyse both the transmission spectrum[55] and energy bands.[54,56] The circular crystal column structure is found to have good optical properties and a large band gap width in the superconducting structure.[57] When the circular crystal column and a square lattice are used as the structure of the two-dimensional superconducting model, the model has a frequency band with a zero transmission spectrum at all angles of incident light. The energy band analysis of the structure reaches the same conclusion on the transmission spectrum, proving the reliability of our study and the promising application prospects of the 2D superconducting network structure in terms of optical properties.

2. Model and methods

The energy bandwidth in PCs is determined by various parameters. In practical optical applications, especially photon detection, we need PCs with wider energy bands to ensure that the same detection performance is realized for photons of different frequencies. In this paper, we explore band broadening methods for HTS PCs while calculating the energy bands of PCs.[58]

All four models used are shown in Table 1. The blue part in the table is the lattice, and the yellow part is the YBCO HTS material. The models in Tables 1(a)–1(c) use a square lattice structure, and that in Table 1(d) uses a triangular lattice structure.[59] In Table 1, a, r, b, c, and d represent the lattice constant, radius of a circular crystal column, side length of a square crystal column, height of a rectangular crystal column, and width of a rectangular crystal column, respectively. The dimensions of the different variables are $a = 2250$ nm–3375 nm, $r = 210$ nm–1190 nm, $b = 280$ nm–2100 nm, $c = 490$ nm–2450 nm, and $d = 420$ nm–1190 nm. The FEM and Floquet periodic boundary conditions are used for modelling and calculation of the different models. For different lattice constants and superconducting material sizes, the photonic band of transverse electric (TE) polarization along the Γ–M direction of the first Brillouin zone is calculated, and the band gaps under different structural parameters and temperatures are analysed.

Table 1. Different superconducting PC structures used in the calculations.

Circular column	Square column	Rectangular column	Circular column
(a) r, a	(b) b, a	(c) c, d, a	(d) r, a

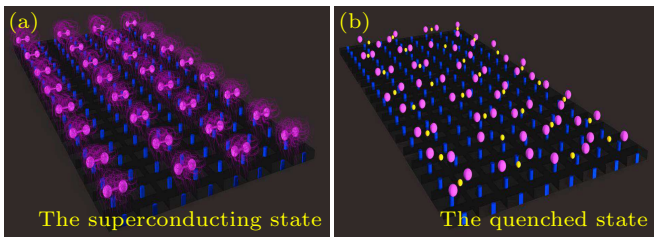


Fig. 1. Schematic diagram of the superconducting state and quenched state models. Subfigure (a) shows the superconducting state, and the refractive index of the material in the superconducting state is studied using the two-fluid model. Subfigure (b) shows the quenched state, and the Drude model is used for refractive index calculation in the quenched state.

Figure 1 shows two-dimensional model diagrams of the superconducting state and quenched state.[60] A blue columnar structure is a superconducting column, and the grey part surrounding the crystal column is a lattice. Purple and yellow spheres are electrons. In Fig. 1(a), electrons exist in the form of Cooper pairs. The refractive index of the material in the superconducting state is studied using the two-fluid model.[61] The electromagnetic response of the superconductor is described by the complex conductivity. In this paper, the loss of the real part of the complex conductivity is neglected, and only the imaginary part of the Cooper pair contribution is considered to calculate the dielectric constant of the material. In the quenched state of Fig. 1(b), electron penetration causes the Cooper pair to break; thus, the electrons exist in a single form, and the superconducting property is lost. Therefore, the Drude model is used for refractive index calculation in the quenched state.

For the above system, we use Maxwell's equations to solve the system properties[22]

$$\nabla \times \frac{1}{\varepsilon(x)} \nabla \times \boldsymbol{E} = \left(\frac{\omega}{c}\right)^2 \boldsymbol{E}, \tag{1}$$

$$\nabla \cdot \boldsymbol{E} = 0. \tag{2}$$

The components of the TE and transverse magnetic (TM) modes can be written as follows:[48]

TE mode

$$-\nabla \cdot \frac{1}{\varepsilon(x)} \nabla \boldsymbol{E} = \left(\frac{\omega}{c}\right)^2 \boldsymbol{E}, \tag{3}$$

TM mode

$$\frac{1}{\varepsilon(x)} \nabla^2 \boldsymbol{E} = \left(\frac{\omega}{c}\right)^2 \boldsymbol{E}, \tag{4}$$

where $\varepsilon(x)$ is the dielectric constant of the material at position x, ω is the frequency, c is the speed of light, and $\boldsymbol{E}$ is the scalar field intensity. The eigenmode obtained by Bloch's theorem is

$$E(x) = \mathrm{e}^{\mathrm{i}\boldsymbol{k}\cdot x} u(x), \tag{5}$$

where $\boldsymbol{k}$ is the Bloch wave vector, and $u(x)$ is the value of the eigenfunction at position x.[47] We compute a set of eigenvalues using different $\boldsymbol{k}$, plotted as a function of $\boldsymbol{k}$ to give a dispersion relation or band diagram.

The relative permittivity of the YCBO material is calculated by the superconducting two-fluid model, London local electrodynamics, and the Drude model. As a result, high-temperature superconductors have optical properties that are distinct from those of conventional materials. Then, the relative permittivity can be calculated by[45,54,60–63]

$$\varepsilon(T,\omega)=\begin{cases}1-\dfrac{1}{\omega^2\mu_0\varepsilon_0\lambda_{\mathrm{L}}^2}, & T<T_{\mathrm{c}},\\ 1-\dfrac{\omega_{\mathrm{p}}^2}{\omega^2+\mathrm{i}\gamma\omega}, & T>T_{\mathrm{c}}.\end{cases}\tag{6}$$

The critical temperature T_{c} of the superconducting material YBCO is 92 K. When temperature T satisfies $T>T_{\mathrm{c}}$ or $T<T_{\mathrm{c}}$, the superconducting material is in the superconducting state or the quenched state, respectively. The relative permittivity of the superconducting material can be calculated using Eq. (6) in different states. ω, μ_0, and ε_0 are the frequency, vacuum permeability, and vacuum permittivity, respectively. λ_{L} is the London penetration depth, calculated by[59]

$$\lambda_{\mathrm{L}}(T)=\frac{\lambda_{\mathrm{L}}(0)}{\sqrt{1-(T/T_{\mathrm{c}})^P}}.\tag{7}$$

The plasma frequency is $\omega_{\mathrm{p}}=1.7\times10^{15}$ rad/s, and the phenomenological damping factor is $\gamma=1.3\times10^{13}$ rad/s.[64,65] The London penetration depth is $\lambda_{\mathrm{L}}(0)=200$ nm when $T=0$ and $P=4$.[60]

For the above models and equations, the FEM is used to analyse the Maxwell equations, and the optical properties of the two-dimensional model are calculated. In this work, we study the properties of HTS PCs from three aspects: maximizing the photonic band gap in a two-dimensional SPC (2D SPC) via different lattices (square lattice and triangular lattice) and different superconducting column structures (circular, square and rectangular), investigating the effects of changing parameters on the band gap width, and studying the effect of incident angle and temperature on the transmission spectrum.[62,66–68]

3. Results and discussion

The 3–5 μm is the mid-infrared band, which is the very important atmospheric window. It has significant applications in the fields of imaging, temperature measurement, early warning, and tracking and in crucial technology developed by various countries. A wide band gap is more favourable for photon detection in our model. The energy

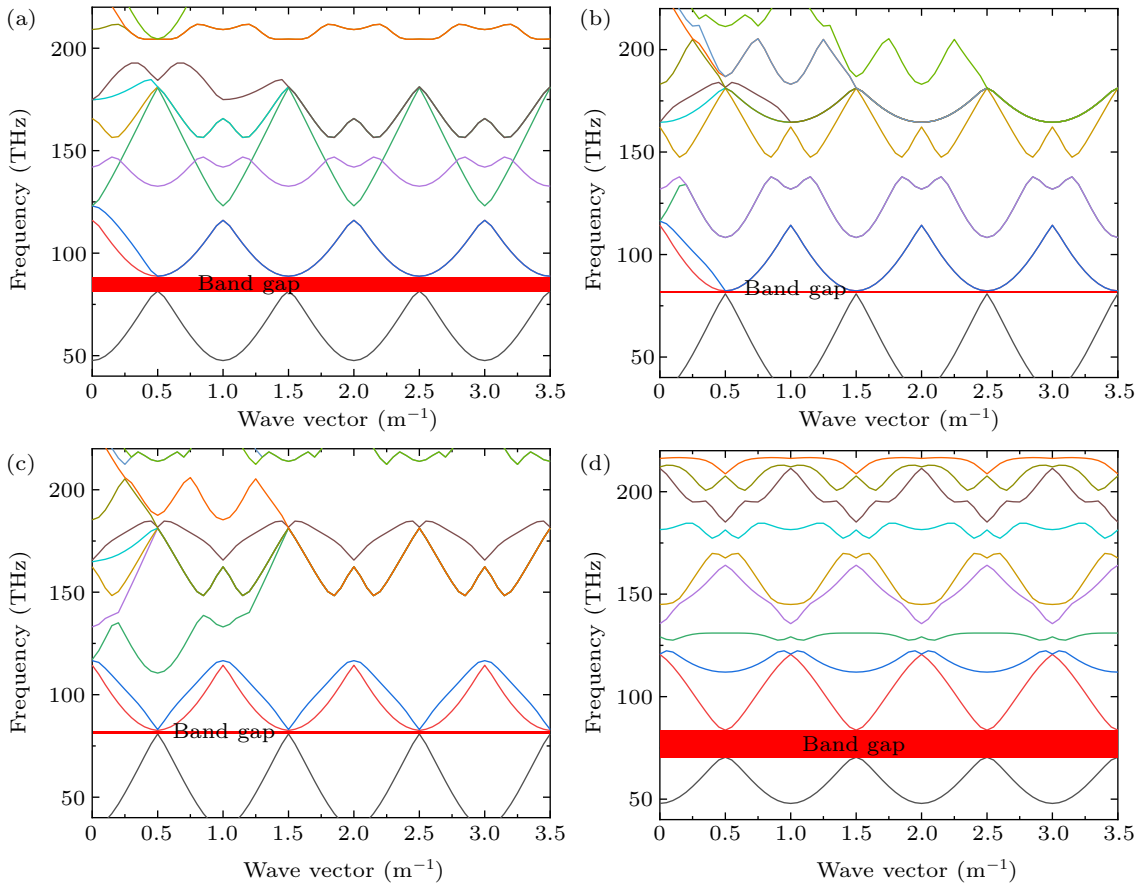


Fig. 2. Energy band diagram of YBCO PCs at different crystal columns and lattices. In subfigures (a)–(c), the lattice structure is square lattice, using circular, square and rectangular superconducting crystal columns, respectively. The structure in subfigure (d) is triangular lattice and circular crystal column. All energy bands are calculated at the temperature of 91 K and the lattice constant $a=2625$ nm. In subfigures (a) and (d), the radius of the crystal column is $r=490$ nm. In subfigure (b), the side length of the square crystal column is $b=490$ nm. In subfigure (c), the height and width of the rectangular crystal column are $c=560$ nm and $d=490$ nm.

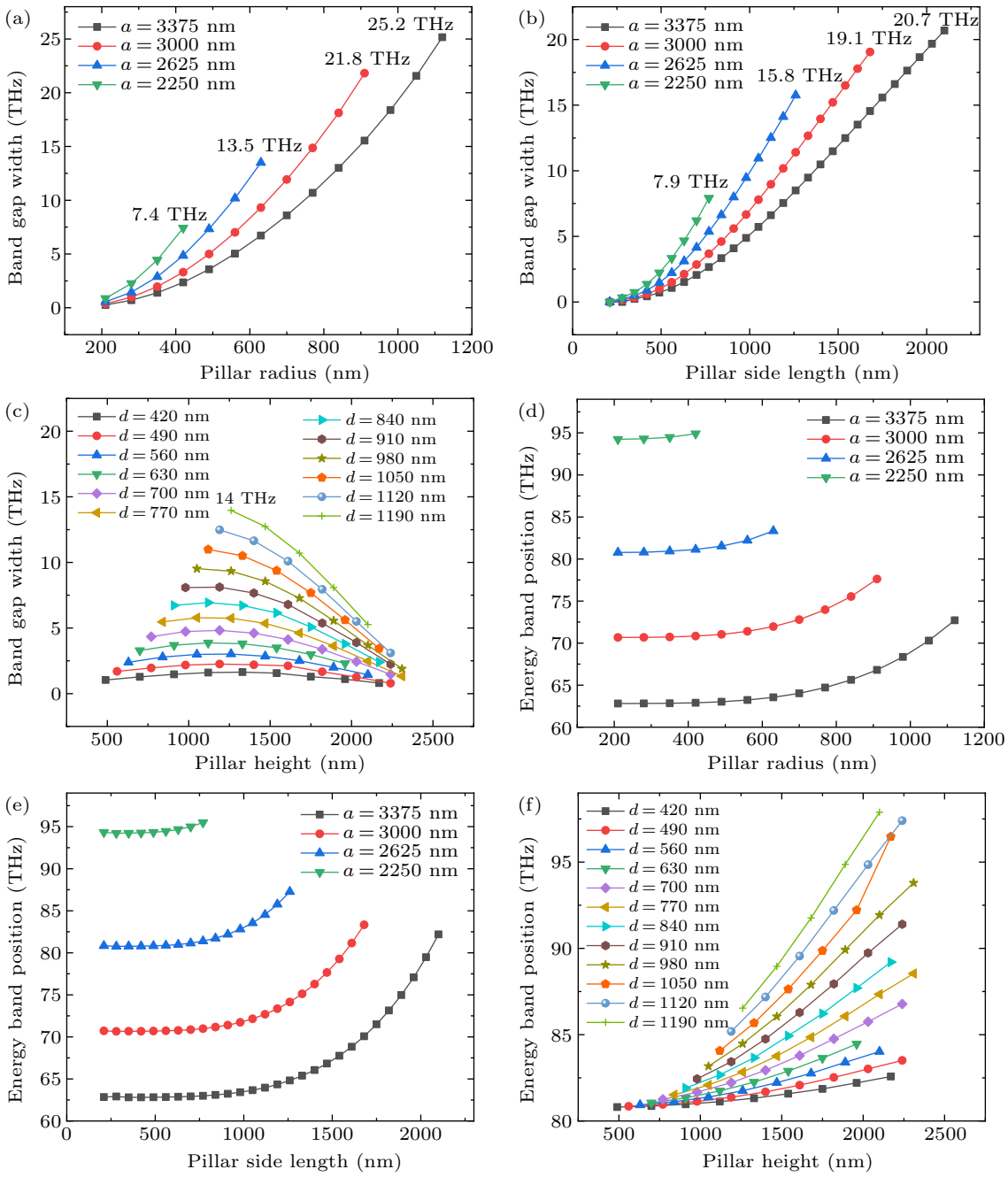


Fig. 3. The band gap width and position of YBCO PCs with different lattice and crystal column structures at $T = 91$ K. Subfigures (a)–(c) show the change of band gap width, in which the crystal columns are circular, square and rectangular. In subfigures (a) and (b), the lattice constants are 2250 nm, 2625 nm, 3000 nm, 3375 nm, and in subfigure (c), the lattice constant is 2625 nm. Subfigures (d)–(f) show the change of the band gap bottom position corresponding to subfigures (a)–(c).

band diagram corresponding to the model in Table 1 is shown in Fig. 2. Two different lattice structures, square and triangle, are used in Figs. 2(a)–2(c) and 2(d). As shown in the red band, each structure has a band gap in the frequency range 60 THz–100 THz (3 μm–5 μm) at $T = 91$ K, $a = 2625$ nm. In Figs. 2(a)–2(c), the parameters are set as $r = 490$ nm, $b = 490$ nm, $c = 560$ nm, and $d = 490$ nm, the bandgap widths are 7.3 THz, 1,47 THz, and 1.69 THz, respectively. In Fig. 2(d), the radius of the circular crystal column is $r = 490$ nm, and the corresponding band gap width is 13.3 THz. We find that different crystal columns and lattice structures have an impact on the band gap width. In order to verify the factors that affect the band gap width, we calculate and analyze different temperature, lattice and crystal column later in the paper.

In this study, the temperature, lattice constant and superconducting column affect the energy band of the system, which in turn affects the bandwidth.[69] Firstly, we study the effects of the lattice constant and superconducting column. Referring to atomic crystals, the properties of the atoms and PCs cells influence the properties of the system, and changing the shape of the columns of the PCs will change the properties of the system. As shown in Fig. 3, we calculate the

band gap widths and positions of the YBCO materials with different shapes at 91 K. As shown in Fig. 3(a), increasing the circular superconducting column size and lattice constant have opposite effects: the band gap width is positively related to the radius of YBCO column and inversely related to the lattice constant. Therefore, to obtain the same band gap, a structure with a larger lattice constant requires a larger YBCO column size. To make the system work in the transparent window of the atmosphere, we limit the energy bandwidth to 3 μm–5 μm, which limits the maximum band gap width that can be achieved with different lattice constants. As shown in Fig. 3(a), the maximum achievable band gap increases from 7.4 THz at $a = 2250$ nm to 25.2 THz at $a = 3375$ nm as the lattice constant changes. The YBCO material in Fig. 3(b) has a square crystal column structure. At different lattice constants, the square pillar size is proportional to the band gap width, which is consistent with the circular crystal column properties. The YBCO material in Fig. 3(c) has a rectangular crystal column structure, and the lattice constant is fixed as $a = 2625$ nm. The different curves and abscissa represent the width d and height c of the rectangular crystal column structure, respectively. In the case of fixed d, the influence of different c on the band gap width is calculated. The band gap width is proportional to d when only d is changed, and a maximum band gap width of 14 THz can be achieved when $d = 1260$ nm. In the case where only c changes, the band gap reaches a maximum value and then decreases. Comparing different lines, we find that the band gap width changes little at 420 nm. The results show that when we need the band gap width does not drastically change with the structure size, we should prepare a width d of 420 nm. Increasing the structure size of the material just to expand the band gap width is unreasonable, and the fill factor of the material should also be considered. Figures 3(d) and 3(f) show the bottom position of the band gap at different lattice constants and crystal columns. In Figs. 3(d) and 3(e), increasing the lattice constant will reduce the lower band gap wavelength limit, and there is a positive correlation between the crystal column size and the band gap position. In Fig. 3(f), we fix the lattice constant as $a = 2625$ nm, and change the width and height of the rectangular crystal column. We find that the band gap position increases with the area of the crystal column. According to the influence of these two parameters, we can adjust the lattice constant and crystal column size to make the band gap appear at the position we need.

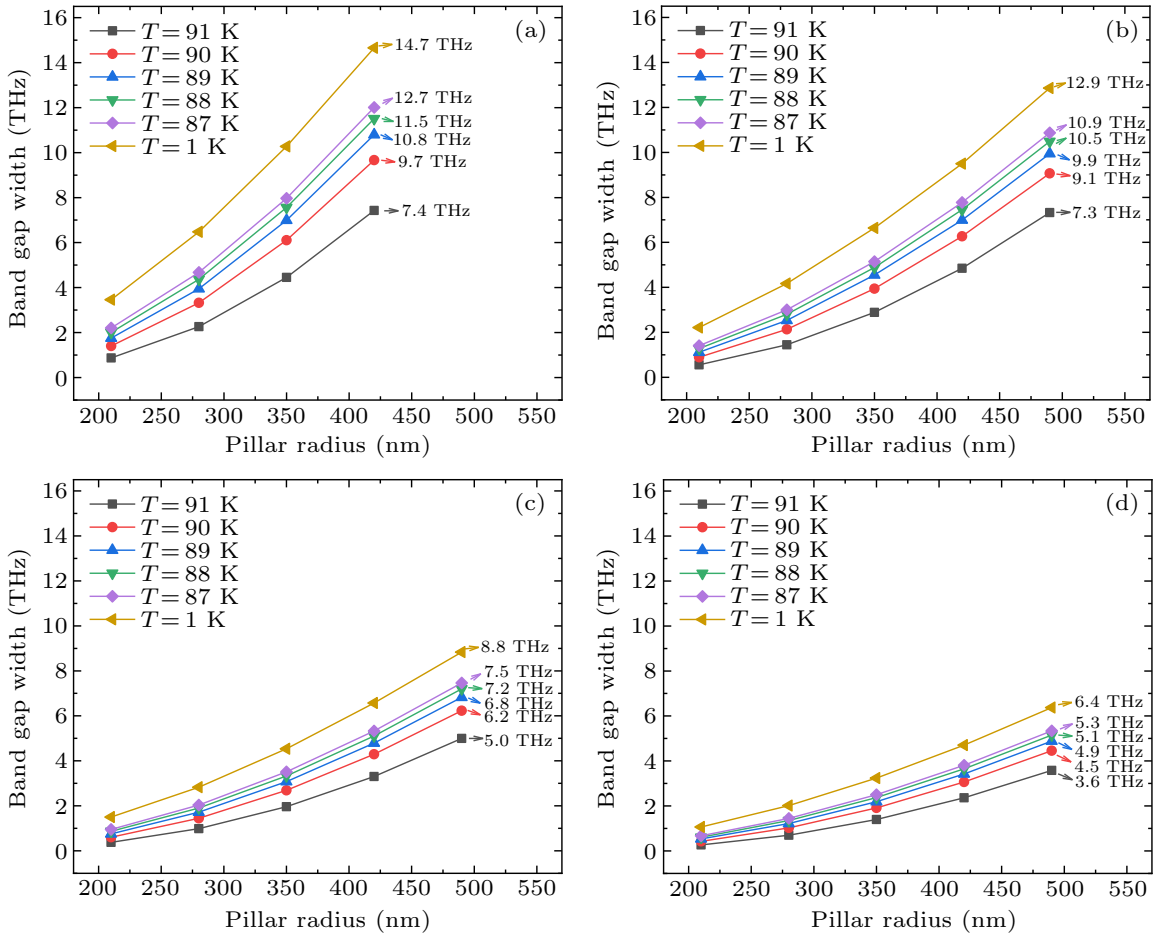


Fig. 4. Band gap widths of YBCO PCs at different temperatures. The column size and bandwidth curves of the YBCO circular crystal column at 91 K–87 K and 1 K are calculated. The lattice constants in each figure are (a) 2250 nm, (b) 2625 nm, (c) 3000 nm, and (d) 3375 nm.

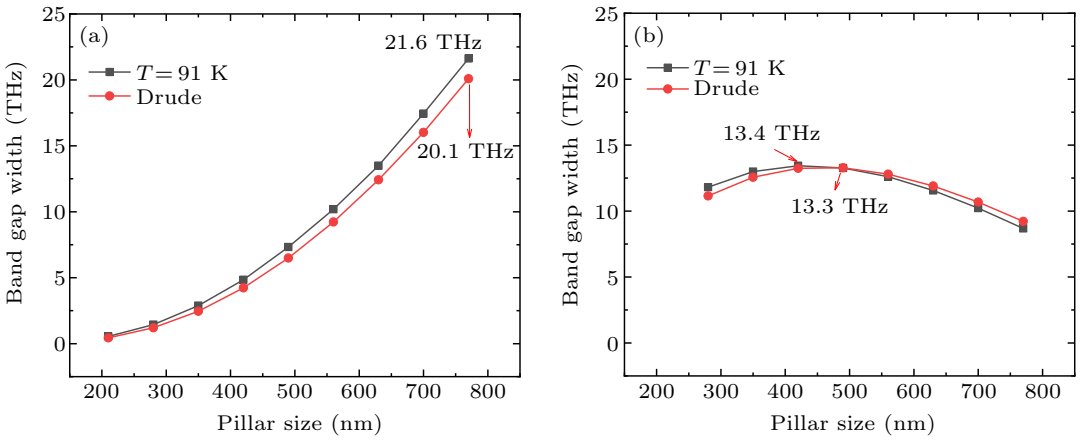


Fig. 5. Band gap widths of superconducting and quenched states with different lattice structures. Subfigure (a) shows the comparison of the band gap widths of superconducting and quenched states in the case of the square lattice. Subfigure (b) shows the comparison of the band gap widths of superconducting and quenched states in the case of the triangular lattice.

Second, we discuss the effect of temperature at different lattice constants. In the superconducting state, as shown in Fig. 4, the band gap width of the system decreases with increasing temperature. For the same band gap value, the higher the temperature of the material is, the larger the pillar size of the material required to maintain the band gap. Under different lattice constants, as shown in Figs. 4(a)–4(d), the change trends of the calculated curves are the same, indicating that the superconducting properties under different lattice constants are stable. When the column size is the same, the larger the lattice constant is, the smaller the band gap width. For example, when the lattice constant is increased from $a = 2625$ nm to 3375 nm, the maximum band gap width decreases from 12.9 THz to 6.4 THz for a column size of $r = 490$ nm at $T = 1$ K.

Many theoretical calculations are based on a square lattice structure. However, in practical applications, most structures cannot achieve the square structure in theory but adopt the arrangement of the triangular lattice structure.[70] In Fig. 5, we compare and analyze the properties and differences of the two lattice structures. Figure 5(a) shows the band gap widths of the system in the superconducting and quenched states when the lattice is square. The width of the band gap in the superconducting state is larger than that in the quenched state, and the bandwidth is positively correlated with the size of the column. The maximum band gap width that can be achieved as 21.6 THz. The lattice in Fig. 5(b) is triangular, with a maximum band gap width of 13.4 THz in the superconducting state, which is slightly larger than that in the quenched state of 13.3 THz. Comparing the variation trends of the band gap width in Figs. 5(a) and 5(b), the triangular lattice is more stable in the change of the superconducting column structure.

For PCs, the fill factor is a parameter related to material utilization, which is defined as

$$f = S_{\text{supercond}}/S_{\text{a}}. \tag{8}$$

After analysing different temperatures, lattice constants and crystal columns, the relationships between the band gap width and fill factor of different crystal column structures are compared. The fill factor is calculated by Eq. (8), where $S_{\text{supercond}}$ is the cross-sectional area of the superconducting crystal column and S_{a} is the lattice cross-sectional area. We show the band gap widths of circular, square and rectangular columns with different fill factors in Fig. 6. The band gap width of circular and square crystal columns is proportional to the fill factor. The slope of the circular crystal column curve is the largest, and at the same fill factor, the band gap will be larger than that of the others crystal columns. When the fill factor of the rectangular column is small, the band gap width is proportional to the fill factor. However, after reaching the maximum band gap width, the band gap width becomes inversely proportional to the fill factor. Since the circular crystal column has the largest band gap width at the same fill factor, the circular crystal column is selected for subsequent calculations and studies.

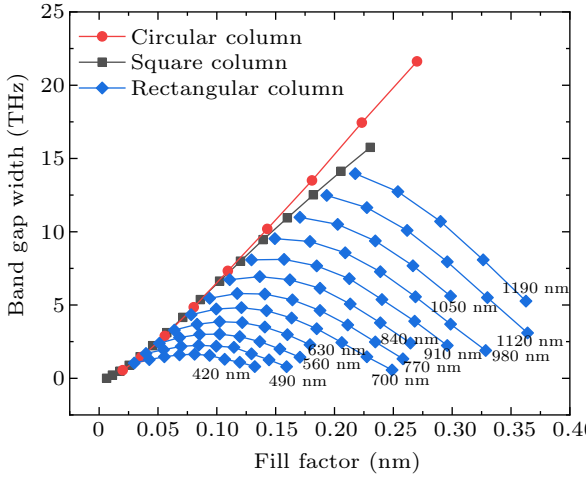


Fig. 6. Fill factor and band gap width curves. The red line corresponds to a circular crystal column, the black curve corresponds to a square crystal column, and the blue curves correspond to rectangular crystal columns with different widths d.

To ensure the accuracy of the calculation, we calculate the

energy bandwidth of the system from the perspective of the transmission spectrum. The transmission spectrum in Fig. 7 is calculated using a square lattice structure with port and Floquet periodic boundary conditions. The changing trends of the transmission spectra at different temperatures and incident angles are analyzed, in which the low part of the transmission spectrum corresponds to the energy gap. In the frequency range of 60 THz–100 THz (3 μm–5 μm), there are zero transmission regions for different incident angles. The temperature in Fig. 7(a) is 91 K, and the width of the zero transmission region is the smallest at 7.5 THz. In Figs. 7(b)–7(f), the width of the zero transmission region expands from 10.1 THz to 13.8 THz as the temperature decreases from 87 K to 1 K. The low transmission spectral part fits well with the band gap width in the band gap curves in Fig. 3(b). We find that there is a good correspondence between the transmission spectrum and the band gap width, which proves that our calculation is scientific and reasonable.

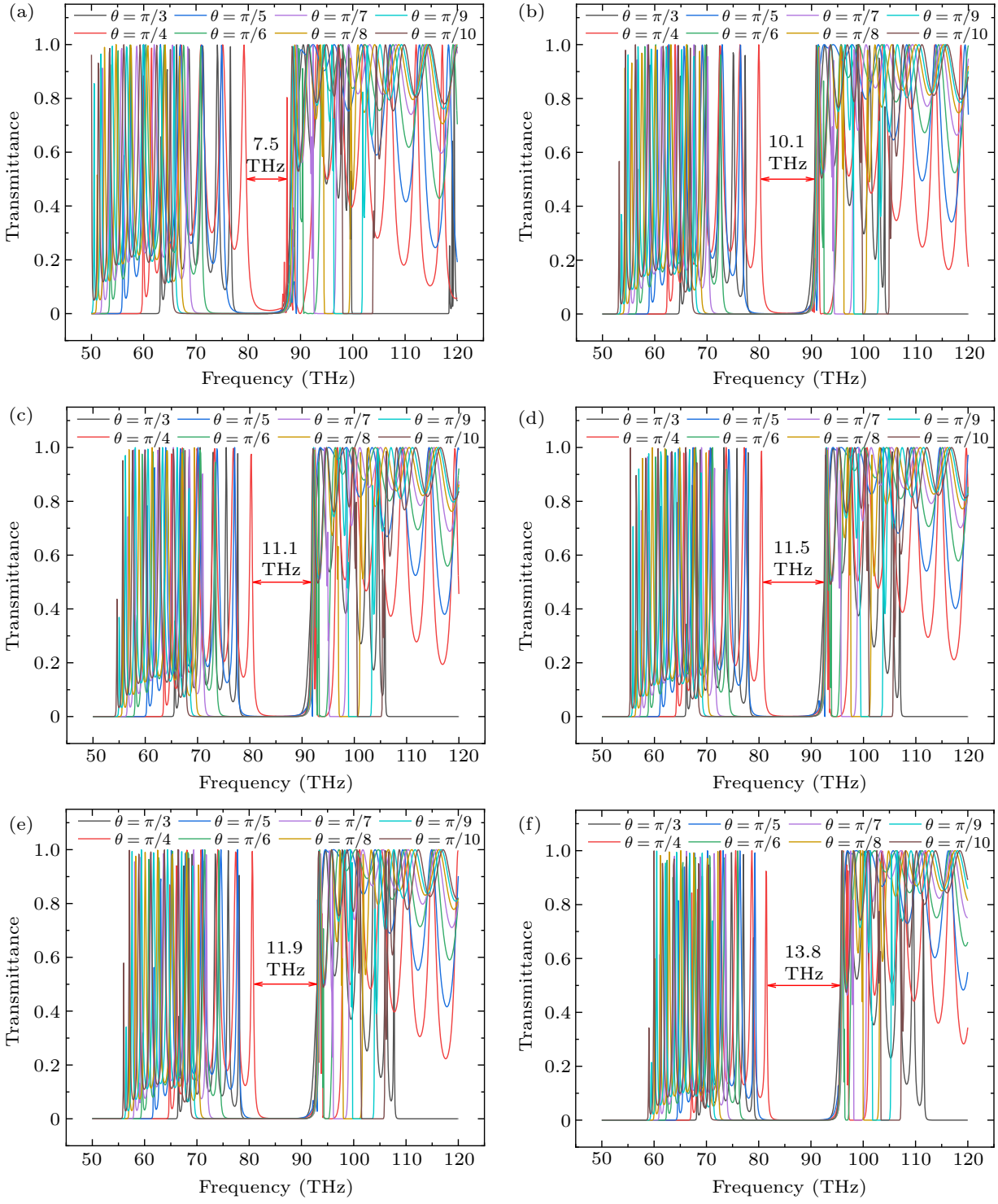


Fig. 7. Transmission spectrum of the two-dimensional square lattice structure. The temperatures in subfigures (a)–(f) are 91 K, 90 K, 89 K, 88 K, 87 K, and 1 K, respectively.

4. Conclusion

We use the FEM to simulate the effects of the superconducting column shape, temperature, lattice constant and lattice arrangement on the band gap width. For different shapes of superconducting columns, the band gap width of circular and square crystal columns is directly proportional to the size of the YBCO column, and there is a maximum band gap width in rectangular crystal columns. For different temperatures, the lower the temperature is, the wider the band gap that can be formed. For different lattice constants, the larger the lattice constant is, the higher the upper limit of the band gap width. For different lattice arrangements, the superconducting band gap width of the square lattice arrangement in the superconducting state is greater than that in the quenched state. A structural change of the superconducting column in the triangular lattice arrangement has little effect on the band gap width, and the performance is more stable. According to the fill factor and band gap width data, a circular crystal column is selected to study the transmission spectrum. At different incident angles and temperatures, the use of square lattice structures results in a zero transmission region in the frequency range of 60 THz–100 THz, and as the temperature decreases, the zero transmission spectral region increases. This study will be beneficial to single-photon detection with 3 μm–5 μm HTSs.

Acknowledgments

Project supported by the National Key Research and Development Program of China (Grant No. 2021YFB3601201), the National Natural Science Foundation of China (Grant No. 62101057), the Fund of State Key Laboratory of Information Photonics and Optical Communications (Beijing University of Posts and Telecommunications) (Grant No. IPOC2021ZT07).

References

[1] Yablonovitch E 1987 *Phys. Rev. Lett.* **58** 2059
[2] John S 1987 *Phys. Rev. Lett.* **58** 2486
[3] Cai Y and Dong Y 2019 *IOP Conf. Ser.: Mater. Sci. Eng.* **473** 012024
[4] Joannopoulos J D, Villeneuve P R and Fan S 1997 *Nature* **386** 143
[5] Yablonovitch E 1994 *J. Mod. Opt.* **41** 173
[6] Threm D, Nazirizadeh Y and Gerken M 2012 *J. Biophotonics* **5** 601
[7] Baker J E, Sriram R and Miller B L 2015 *Lab Chip* **15** 971
[8] Rifat A A, Mahdiraji G A and Ahmed R 2015 *IEEE Photon. J.* **8** 4800408
[9] Li L, Li T and Ji F 2017 *Microsyst. Technol.* **23** 3271
[10] Xia J, Qiao Q and Zhou G 2020 *Appl. Sci.* **10** 7080
[11] Choi H Y, Park K S and Park S J 2008 *Opt. Lett.* **33** 2455
[12] Hameed M F O, Azab M Y and Heikal A M 2015 *IEEE Photon. Technol. Lett.* **28** 59
[13] Chu S, Olmedo M and Yang Z 2008 *Appl. Phys. Lett.* **93** 181106
[14] Wu D K C, Kuhlmey B T and Eggleton B J 2009 *Opt. Lett.* **34** 322
[15] Goyal A K, Dutta H S and Pal S 2017 *J. Phys. D: Appl. Phys.* **50** 203001
[16] Xu H, Wu P and Zhu C 2013 *J. Mater. Chem. C* **1** 6087
[17] Schmidt M A, Argyros A and Sorin F 2015 *Adv. Opt. Mater.* **4** 13
[18] Russell P 2003 *Science* **299** 358
[19] Skivesen N, Têtu A and Kristensen M 2007 *Opt. Express* **15** 3169
[20] Bao J, Xiao J and Fan L 2014 *Opt. Commun.* **329** 109
[21] Dutta H S, Goyal A K and Srivastava V 2016 *Photon. Nanostruct.* **20** 41
[22] Song G Z, Munro E and Nie W 2018 *Phys. Rev. A* **98** 023814
[23] Song G Z, Zhang M and Ai Q 2017 *Ann. Phys.* **378** 33
[24] Yang D, Wang C and Ji Y 2016 *Opt. Express* **24** 16267
[25] Costa R, Melloni A and Martinelli M 2003 *IEEE Photon. Technol. Lett.* **15** 401
[26] Mahmoud M Y, Bassou G and Taalbi A 2012 *Opt. Commun.* **285** 368
[27] Rezaee S, Zavvari M and Alipour-Banaei H 2015 *Optik* **126** 2535
[28] Wang T J, Song S Y and Long G L 2012 *Phys. Rev. A* **85** 062311
[29] Ren B C and Long G L 2014 *Opt. Express* **22** 6547
[30] Xu X S, Zhang H and Kong X Y 2020 *Photon. Res.* **8** 490
[31] Münzberg J, Vetter A and Beutel F 2018 *Optica* **5** 658
[32] Vetter A, Ferrari S and Rath P 2016 *Nano Lett.* **16** 7085
[33] Zhang W J, Li H and You L X 2016 *IEEE Photon. J.* **8** 1
[34] Zhang L, Gu M and Jia T 2014 *IEEE Photon. J.* **6** 1
[35] Yang C, Liu H and Liu Y 2022 *Nature* **601** 205
[36] Yang C, Liu Y and Wang Y 2019 *Science* **366** 1505
[37] Pedarnig J D, Bodea M A and Steiger B 2012 *Phys. Procedia* **36** 508
[38] Aly A H, Ghany S E S A and Kamal B M 2020 *Ceram. Int.* **46** 365
[39] Thapa K B, Srivastava S and Tiwari S 2010 *J. Supercond. Nov. Magn.* **23** 517
[40] Berman O L, Lozovik Y E and Eiderman S L 2006 *Phys. Rev. B* **74** 092505
[41] Qiu D, Gong C and Wang S S 2021 *Adv. Mater.* **33** 2006124
[42] Ooi C H R, Yeung T C A and Kam C H 2000 *Phys. Rev. B* **61** 5920
[43] Aly A H and Mohamed D 2015 *J. Supercond. Nov. Magn.* **28** 1699
[44] Lin W H, Wu C J and Yang T J 2010 *Opt. Express* **18** 27155
[45] Kumar A R, Zhang Z M and Boychev V A 1999 *J. Heat Transfer* **121** 844
[46] Rifat A A, Mahdiraji G A and Chow D M 2015 *Sensors* **15** 11499
[47] Fietz C, Urzhumov Y and Shvets G 2011 *Opt. Express* **19** 19027
[48] Hiett B P, Generowicz J M and Cox S J 2002 *IEE Proc. Sci. Meas. Technol.* **149** 293
[49] Boffi D, Conforti M and Gastaldi L 2006 *Numer. Math.* **105** 249
[50] Yang D, Gao F and Cao Q T 2018 *Photon. Res.* **6** 99
[51] Qi Y P, Wang L Y and Zhang Y 2020 *Chin. Phys. B* **29** 067303
[52] Meng J, Hou L T and Zhou G Y 2008 *Chin. Phys. B* **17** 3779
[53] Hao K S, Huang S L and Zhao W 2011 *Chin. Phys. B* **20** 068104
[54] El-Naggar S A, Elsayed H A and Aly A H 2014 *J. Supercond. Nov. Magn.* **27** 1615
[55] Aly A H 2009 *Chem. Phys.* **115** 391
[56] Axmann W and Kuchment P 1999 *J. Comput. Phys.* **150** 468
[57] Aly A H, Elsayed H A and El-Naggar S A 2014 *J. Mod. Opt.* **61** 1064
[58] Villeneuve P R and Piche M 1994 *Quantum Electron.* **18** 153
[59] Diaz-Valencia B F and Calero J M 2017 *J. Low Temp. Phys.* **186** 275
[60] Zamani M 2016 *Phys. C* **520** 42
[61] Van Duzer T and Turner C W 1981 *Phys. Today* **35** 80
[62] Degirmenci E and Landais P 2013 *Appl. Opt.* **52** 7367
[63] Zhao Y and Grischkowsky D R 2007 *IEEE Trans. Microw. Theor. Tech.* **55** 656
[64] Hu C, Zhang H and Liu G 2019 *Appl. Opt.* **58** 2890
[65] Chang T W, Huang C H and Hou D J 2017 *IEEE Photon. J.* **9** 1
[66] Song G Z, Kwek L C and Deng F G 2019 *Phys. Rev. A* **99** 043830
[67] Baraket Z, Zaghdoudi J and Kanzari M 2017 *Opt. Mater.* **64** 147
[68] Wu J and Gao J 2015 *Optik* **126** 5368
[69] Elsayed H A, El-Naggar S A and Aly A H 2014 *J. Mod. Opt.* **61** 385
[70] Fathollahi Khalkhali T and Bananej A 2017 *J. Mod. Opt.* **64** 830